AIAA JOURNAL
Vol. 50, No. 12, December 2012

Further Studies of Airfoils Supporting Non-Unique Solutions in Transonic Flow

Antony Jameson*
Stanford University, Stanford, California 94305
John C. Vassberg†
The Boeing Company, Huntington Beach, California 92647
and
Kui Ou‡
Stanford University, Stanford, California 94305

DOI: 10.2514/1.J051713

Non-unique solutions of the Euler equations were originally discussed by Jameson in 1991 ("Airfoil Admitting Non-Unique Solutions to the Euler Equations," AIAA Paper 1991-1625, June 1991) for several highly cambered airfoils which were the result of aggressive shape optimization. In 1999 Hafez and Guo ("Nonuniqueness of Transonic Flows," *Acta Mechanica*, Vol. 138, Nos. 3–4, 1999, pp. 177–184) found non-unique solutions for a symmetric parallel sided airfoil, and subsequently Kuz'min and Ivanova ("The Structural Instability of Transonic Flow Associated with Amalgamation/Splitting of Supersonic Regions," *Theoretical and Computational Fluid Dynamics*, Vol. 18, No. 5, 2004, pp. 335–344) have discovered some fully convex symmetric airfoils that provide non-unique solutions. In this article four new symmetric airfoils, all of which exhibit non-unique solutions in a narrow band of transonic Mach numbers, are studied. The first, NU4 was the result of shape optimization. The second, JF1 is an extremely simple parallel sided airfoil. The third JB1, is also parallel sided but has continuous curvature over the entire profile. The fourth, JC6, is convex and C_∞ continuous. $C_L - \alpha$ plots of these airfoils exhibit three branches at zero angle of attack, the *P*-, *Z*- and *N*-branches with positive, zero and negative lift respectively. At some Mach numbers no stable *Z*-branch could be found. When the *P*-branch is continued to negative α in some cases there is a transition to the *Z*-branch, while in other cases there is a direct transition from the *P*- to the *N*-branch.

I. Introduction

GIVEN that the equations governing steady inviscid compressible flow are nonlinear, one can anticipate the possibility of non-unique solutions. A familiar example is the case of supersonic flow past a wedge at an angle θ, in which there are two solutions with different shock angles β corresponding to the strong and weak branches of the $\beta - \theta$ diagram. Non-unique solutions of the transonic potential flow equation were discovered by Steinhoff and Jameson [1], who obtained lifting solutions for a symmetric Joukowski airfoil at zero angle of attack in a narrow range of Mach numbers in the neighborhood of Mach 0.85. This non-uniqueness could not be duplicated with the Euler equations, and it was conjectured by Salas et al. [2] that the non-uniqueness was a consequence of the isentropic flow approximation. Subsequently, however, Jameson [3] discovered several airfoils that supported non-unique solutions of the Euler equations in a narrow Mach band. These airfoils were lifting.

The question of non-unique transonic flows was re-examined by Hafez and Guo [4–6] who formed both lifting and non-lifting solutions for a 12-percent-thick symmetric airfoil with parallel sides from 25 to 75% chord in a Mach range from 0.825 to 0.843. The question was further pursued in detail in a series of studies by Kuz'min and Ivanova [7–11], who confirmed the results of Hafez and Guo and also showed that airfoils with positive curvature everywhere could support non-unique solutions.

Presented at the 29th AIAA Applied Aerodynamics Conference , Honolulu, Hawaii, June 27–30, 2011; received 1 November 2011; revision received 8 March 2012; accepted for publication 29 March 2012.

*Thomas V. Jones Professor, Aeronautics and Astronautics Department. Fellow AIAA.
†Boeing Technical Fellow, Phantom Works. Fellow AIAA.
‡Ph.D. Candidate, Aeronautics and Astronautics Department, Student Member AIAA.

II. Problem Statement

A. NU4 Airfoil

The present authors have encountered another example as a consequence of a shape optimization study for symmetric airfoils in transonic flow [12], in which an attempt was made to find a 12-percent-thick airfoil with a shock-free solution at Mach 0.84. The resulting airfoil, labelled NU4, has an almost shock-free solution at its designated Mach number, but it also allows a lifting and non-lifting solution at zero angle of attack. To better understand this phenomenon, three other approximately 12-percent-thick symmetric airfoils have been analyzed in detail.

B. JF1 Airfoil

The first, the JF1 airfoil, is even simpler than the shape proposed by Hafez and Guo [4], consisting of a parallel-sided slab closed by a semicircular nose and two parabolic arcs at the rear. Depending on the extent of the parabolic arcs, a Mach range exists in which lifting solutions can be found at zero angle of attack.

C. JB1 Airfoil

The second, the JB1 airfoil, also has a parallel center section but the nose and tail are closed by higher-order curves that maintain continuity of the curvature at the junction points. The nose section is defined by a Bezier curve with the following four control points:

$$x_1 = 0, \quad y_1 = 0 \quad x_2 = 0, \quad y_2 = 1 \quad x_3 = 1,$$
$$y_3 = 1 \quad x_4 = 1, \quad y_4 = 1$$

scaled to a length of 0.125 and a height of 0.0625. The upper surface curve is defined by

$$x = 0.125(3t^2 - 2t^3) \qquad y = 0.0625(3t - 3t^2 + t^3), \qquad 0 \le t \le 1$$

The trailing curve from $x = 0.625$ to 1 is

$$y = 0.0625\left\{1 - \left[1 - \left(\frac{1-x}{0.375}\right)\right]^3\right\}$$

D. JC6 Airfoil

The third airfoil, JC6, is a fully convex airfoil defined by a simple algebraic formula:

$$y(x) = Cx^{\frac{1}{n}}(1 - x^n), \qquad 0 \le x \le 1$$

where the constant C, with a value of 0.06817, is adjusted to give the specified maximum thickness, 12% of the chord. The choice $n = 6$ results in a very blunt-nosed airfoil with maximum thickness at about 55% of the chord, which has positive curvature everywhere and is C_∞ continuous.

E. Overview

These four airfoils have very different characteristics, but they all share the property that in non-lifting transonic flow they exhibit a transition from a solution with two supersonic zones on each surface below a certain critical Mach number to a solution with one supersonic zone on each surface above the critical Mach number. In the region of instability, solutions with positive lift are found in which there is a single supersonic zone on the top surface and two supersonic zones on the lower surface, and also solutions with negative lift that are the mirror images of the solutions with positive lift. There results are presented in more detail in the next section.

III. Results

The calculations for the first three airfoils were performed using the authors' SYN83 code, which implements the Jameson–Schmidt–Turkel scheme [13] on a mesh with C-topology. The mesh contained 384 cells in the clockwise direction and 64 cells in the normal

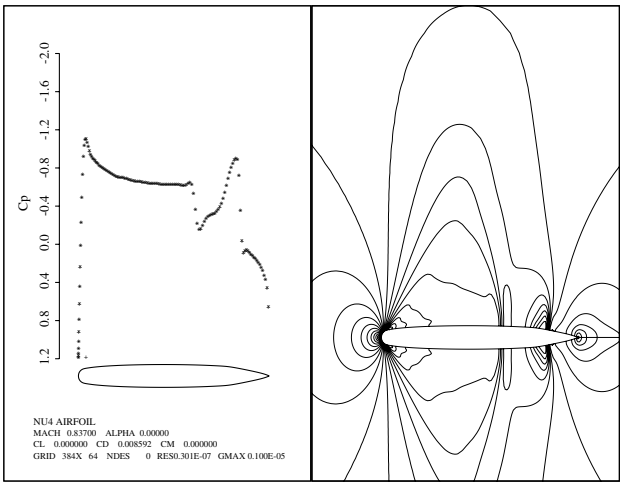

a) Z-branch Cp distribution and mach contours

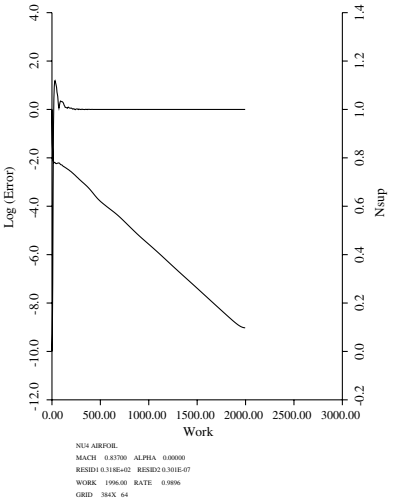

b) Z-branch convergence history

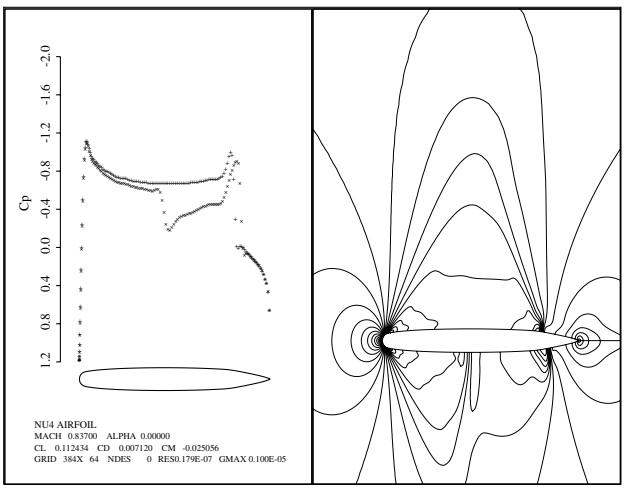

c) P-branch Cp distribution and mach contours

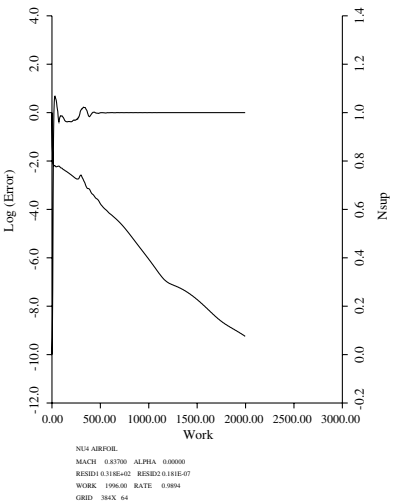

d) P-branch convergence history

Fig. 1 NU4 at Mach = 0.837 showing the symmetric solution (a) and convergence history (b), and the asymmetric solution (c) and convergence history (d).

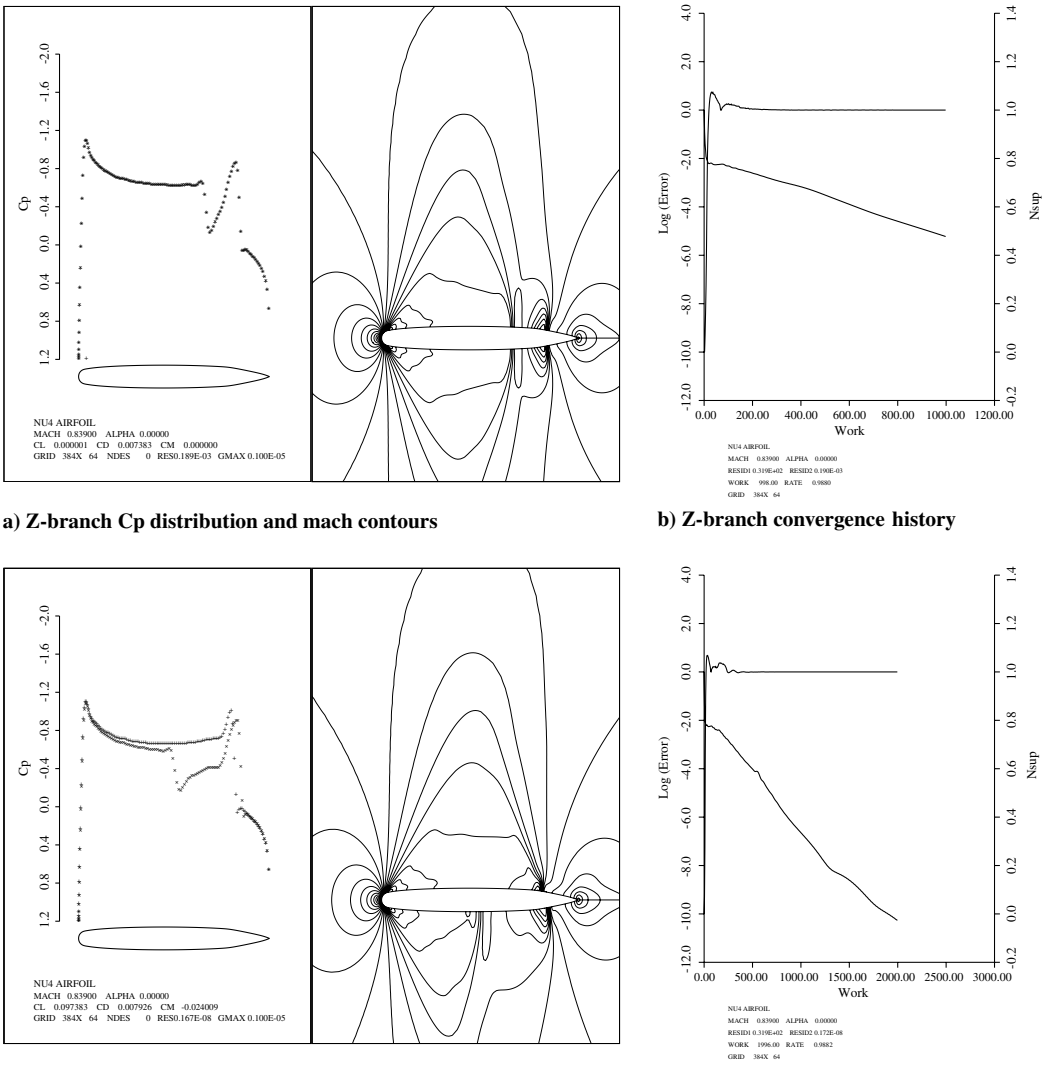

a) Z-branch Cp distribution and mach contours

b) Z-branch convergence history

c) P-branch Cp distribution and mach contours

d) P-branch convergence history

Fig. 2 NU4 at Mach = 0.839 showing the symmetric solution (a) and convergence history (b), and the asymmetric solution (c) and convergence history (d).

direction. In all cases, a lifting solution at zero angle of attack was obtained by starting at an angle of attack of 0.005 deg and switching to 0 deg after 500 iterations. The corresponding negative lifting solution can be obtained by starting at −0.005 deg and is the exact mirror image.

A. NU4 Airfoil

Examining first the NU4 airfoil, stable asymmetric solutions were found in the range of Mach numbers from 0.837 to 0.841. As the Mach number is increased, there is a progressively decreasing distance between the two supersonic zones on the lower surface (in the case of positive lift). This is illustrated in Figs. 1–3. At Mach 0.841, the symmetric solution is close to shock-free, with a single relatively weak shock.

B. JF1 Airfoil

Examining next the JF1 airfoil, which is closed at the rear by parabolic arcs from 76% chord, non-unique solutions were found in the range of Mach numbers from 0.825 to 0.835, illustrated in Figs. 4–6. Figures 4a and 4c show the symmetric and positive lifting solutions at Mach 0.825, respectively, together with their convergence histories. Figures 5 and 6 show the corresponding results at Mach 0.830 and 0.835, respectively. As the Mach number is increased, the double shock zone becomes narrower. When it becomes too narrow above Mach 0.835 or too wide below Mach 0.825, the initial lifting solution at 0.005 deg decays when the angle of attack is reduced to zero. It may also be observed that the symmetric solutions at Mach 0.825 and 0.830 started to diverge after reaching extremely low values of the residual of the order of 10^{-12} and 10^{-11}, respectively, at around 1500 cycles, suggesting that at these Mach numbers the symmetric solution may not be a stable equilibrium point. SYN83 uses a multigrid solution procedure, in combination with variable local time steps and residual averaging. These procedures could possibly stabilize an unstable solution, and so time-accurate simulations will be needed to assess the true stability of the symmetric solutions.

C. JB1 Airfoil

The JB1 airfoil differs from the JF1 airfoil primarily in maintaining continuity of the curvature over the entire profile and having a slightly larger thickness of 12.5%. Nevertheless, the results displayed in Figs. 7–9 have a very similar character, with non-unique solutions in a somewhat narrower range of Mach numbers from 0.823 to 0.827.

D. JC6 Airfoil

Corresponding results for the JC6 airfoil are shown in Figs. 10–12. In these cases, stable asymmetric solutions were formed in the range

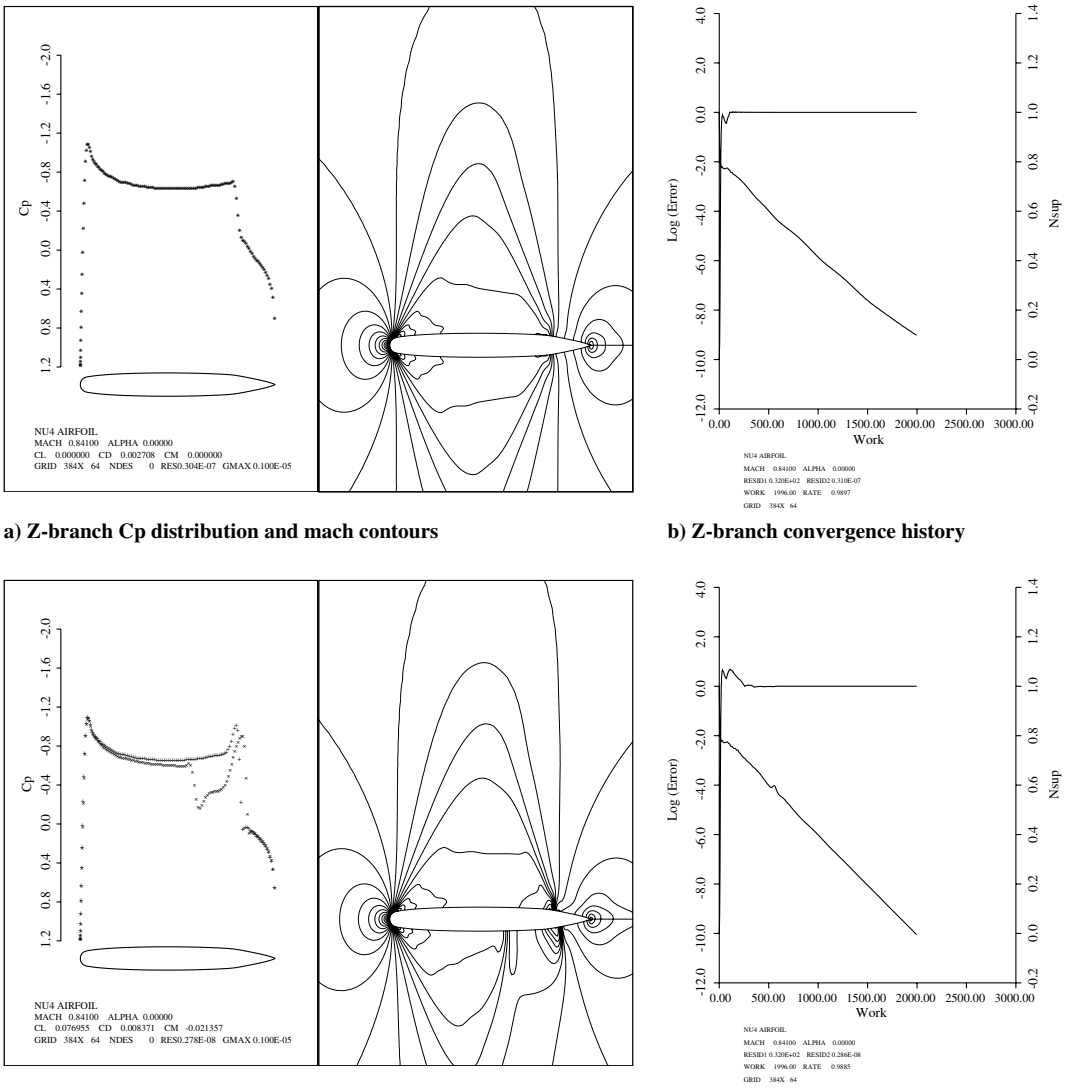

a) Z-branch Cp distribution and mach contours

b) Z-branch convergence history

c) P-branch Cp distribution and mach contours

d) P-branch convergence history

Fig. 3 NU4 at Mach = 0.841 showing the symmetric solution (a) and convergence history (b), and the asymmetric solutions (c) and convergence history (d).

of Mach numbers from 0.844 to 0.848. These calculations were also performed with SYN83, but because of the extreme blunt nose shape of this airfoil, a finer mesh with 768×128 cells was used. The general character of the solutions is similar to that of the JF1 airfoils, confirming that non-unique solutions can be found for an extremely smooth convex profile with positive curvature everywhere. To verify that these solutions are not a consequence of the mesh or the discretization scheme, this airfoil was also analyzed on an O-mesh with 512×512 cells with an uniform aspect ratio of unity. Figure 13 illustrates a corresponding mesh with 128×128 cells. Calculations were performed using a version of the authors' FLO82 code, which implements the H-CUSP scheme [14], and with NASA's Overflow code [15]. The results confirmed the same trend. Figure 14 shows the three solutions for Mach 0.847 at zero angle of attack calculated using FLO82.

E. Plots of $C_L - \alpha$ Sweeps

To further elucidate the behavior, C_L versus α curves were calculated for all four airfoils at the Mach number where they exhibit non-unique solutions. Overall, three different regimes can be identified as the Mach number is varied over a narrow band. Typically, the $C_L - \alpha$ curve has three branches with zero, positive, and negative lift at zero angle of attack (the *Z*-, *P*-, and *N*-branches). In the first regime, there appears to be no stable solution at zero angle of attack, although it may be possible to force convergence to very small values of the error residual. In this case there is no *Z*-branch. The *P*-branch can be continued to negative angles of attack before there is a transition directly to the *N*-branch. In the second regime, there is a *Z*-branch in which stable solutions are found over a small range of angle of attack. However, when the *P*-branch is continued to negative α there is eventually a direct transition to the *N*-branch. In the third regime there is a larger *Z*-branch, and when the *P*-branch is continued to negative α, there is a transition to the *Z*-branch, and then as α is further reduced to a more negative value, there is a second transition to the *N*-branch. These regimes can be seen for the different airfoils in Figs. 15–18. Figure 15 shows the NU4 airfoil at Mach 0.840. It exhibits the third behavior, with a transition from the *P*- to the *N*-branch via the *Z*-branch. Figure 16 shows that the JF1 airfoil has a similar behavior at Mach 0.835. The lower figure is a zoom of the upper picture. Figure 17 shows the JB1 airfoil at Mach 0.827. This shows the second regime where there is a direct transition from the *P*- to the *N*-branch. At Mach 0.825, no stable *Z*-branch could be found for this airfoil, indicating that it is in the first regime. Figure 18 shows that the JC6 airfoil is in the second regime at Mach 0.847. In this case the $C_L - \alpha$ sweep was calculated on 512×512 O-mesh using both FLO82-HCUSP and Overflow, to verify the behavior. To better understand the stability of these solutions, time-accurate

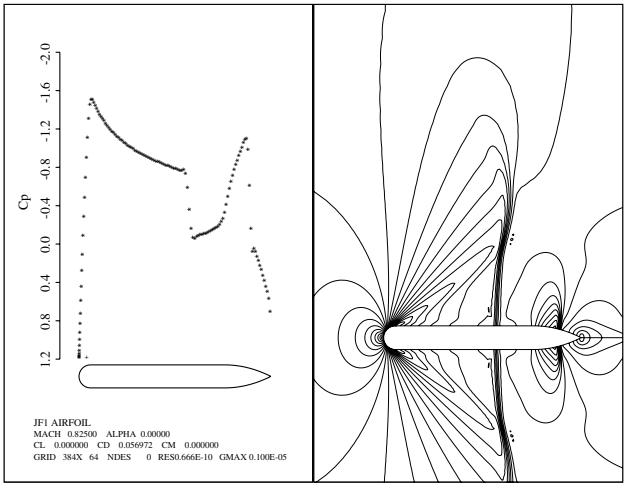

a) Z-branch Cp distribution and mach contours

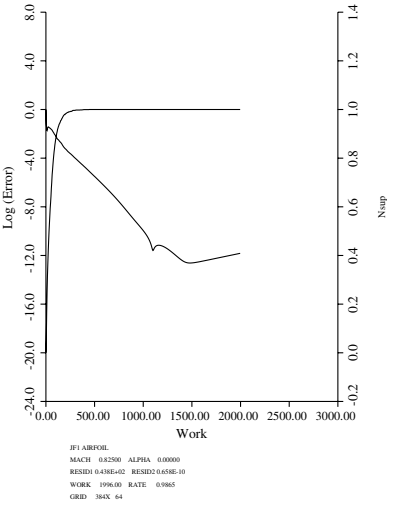

b) Z-branch convergence history

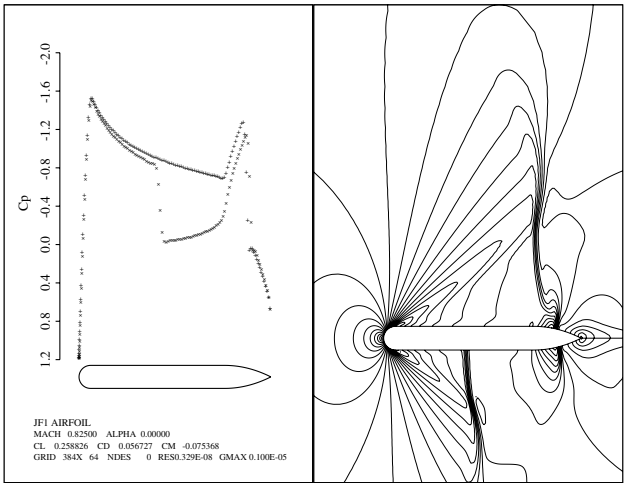

c) P-branch Cp distribution and mach contours

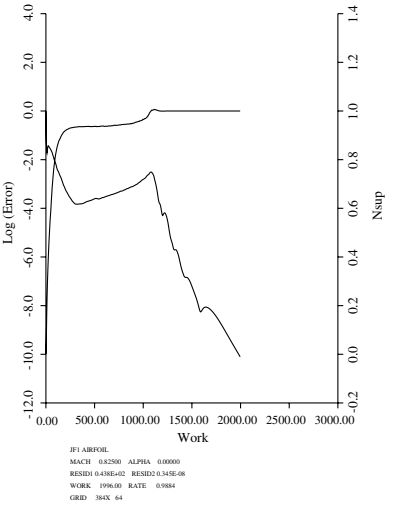

d) P-branch convergence history

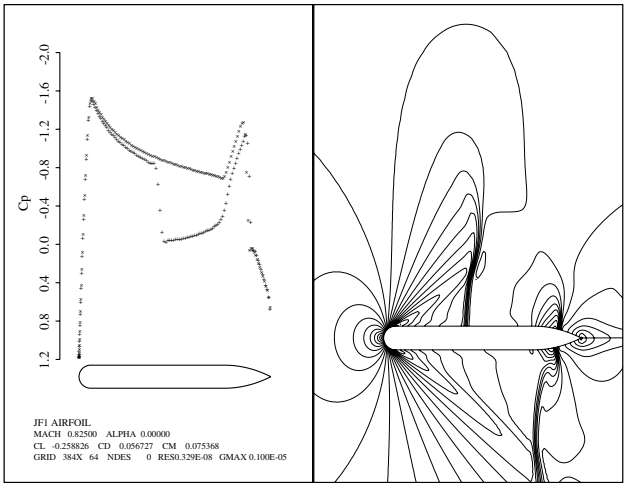

e) N-branch Cp distribution and mach contours

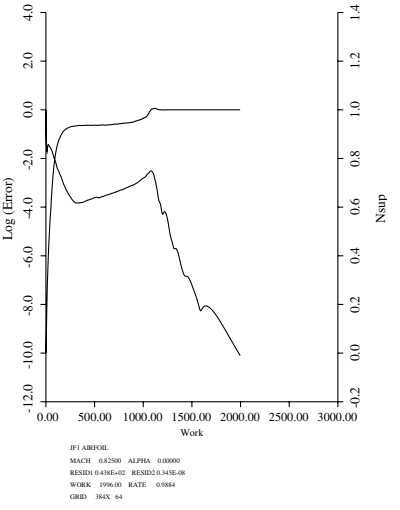

f) N-branch convergence history

Fig. 4 JF1 at Mach = 0.825 showing the symmetric solution (a) and convergence history (b), and the pair of asymmetric solutions (c and e) and convergence histories (d and f).

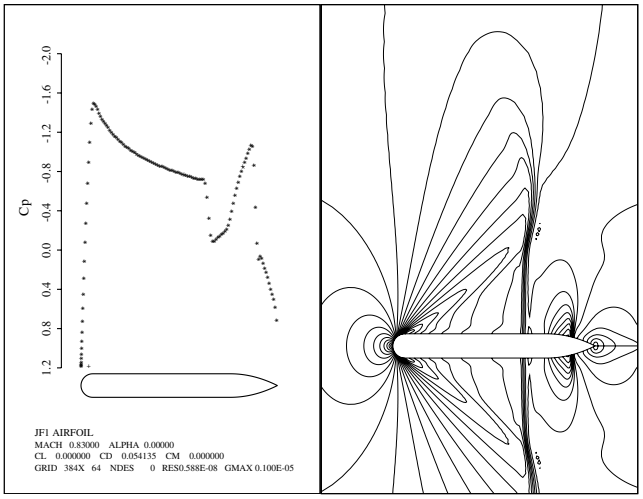

a) Z-branch Cp distribution and mach contours

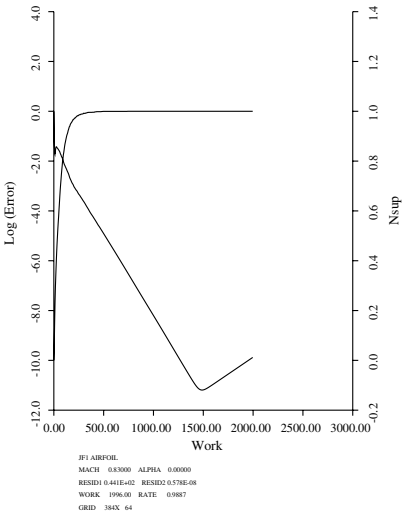

b) Z-branch convergence history

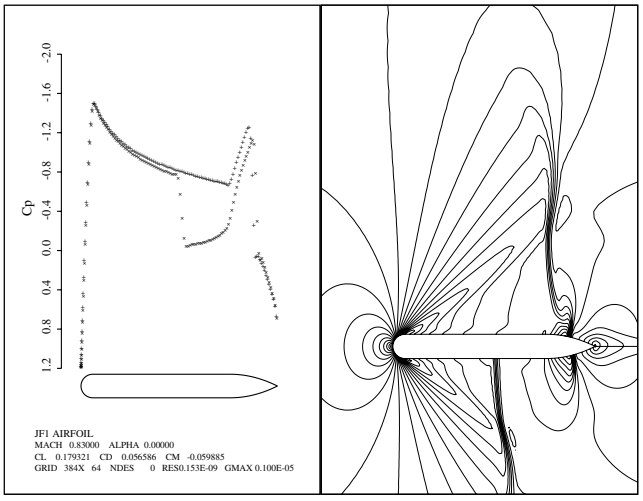

c) P-branch Cp distribution and mach contours

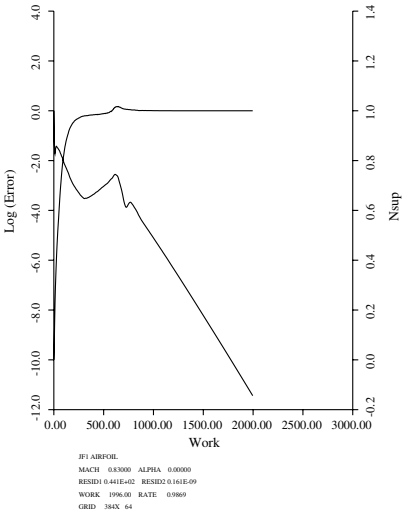

d) P-branch convergence history

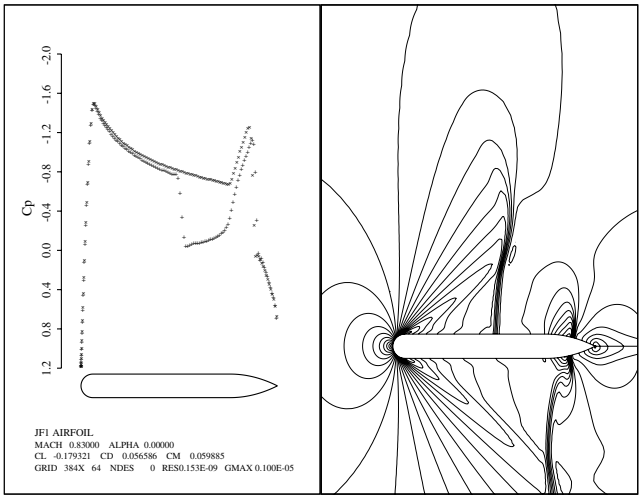

e) N-branch Cp distribution and mach contours

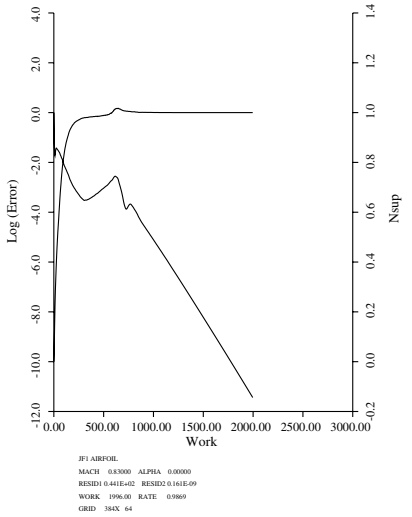

f) N-branch convergence history

Fig. 5 JF1 at Mach = 0.830 showing the symmetric solution (a) and convergence history (b), and the pair of asymmetric solutions (c and e) and convergence histories (d and f).

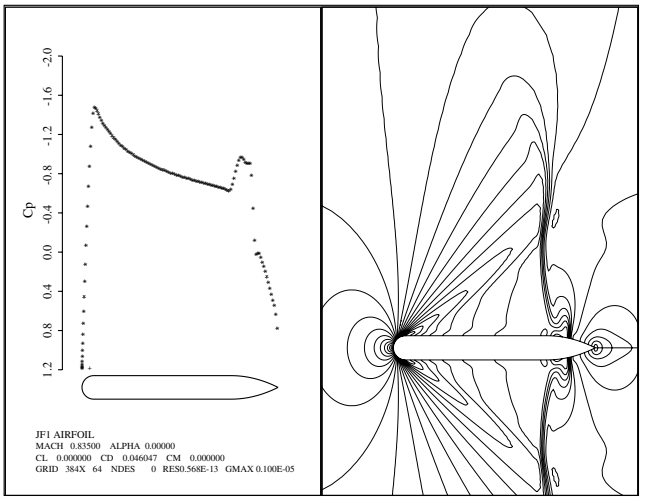

a) Z-branch Cp distribution and mach contours

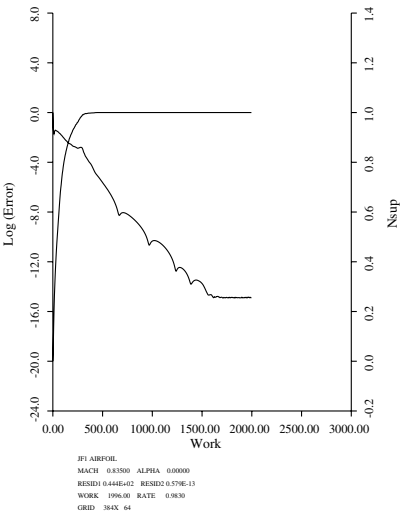

b) Z-branch convergenc history

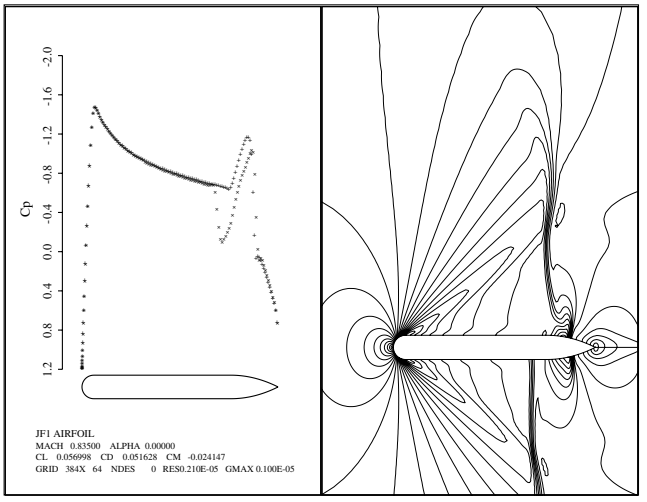

c) P-branch Cp distribution and mach contours

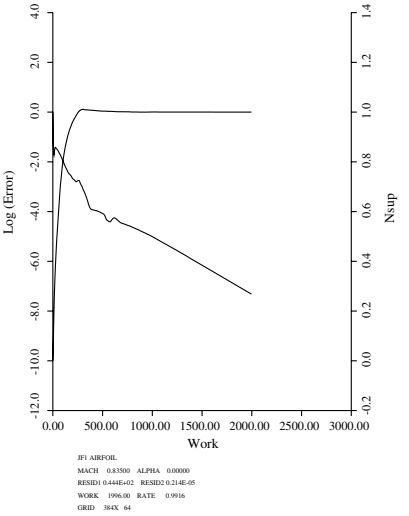

d) P-branch convergencehistory

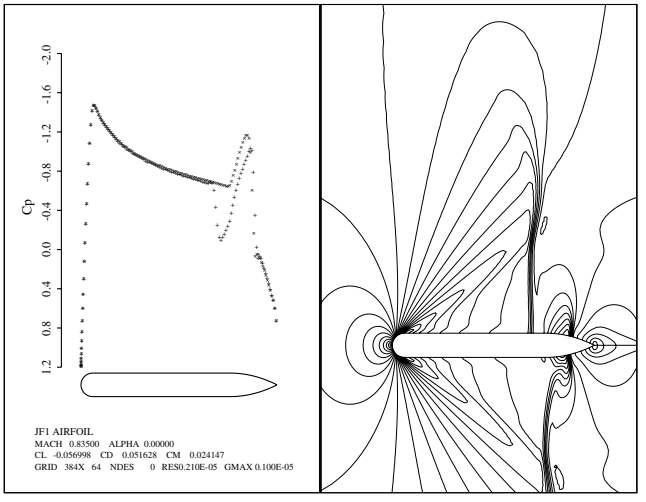

e) N-branch Cp distribution and mach contours

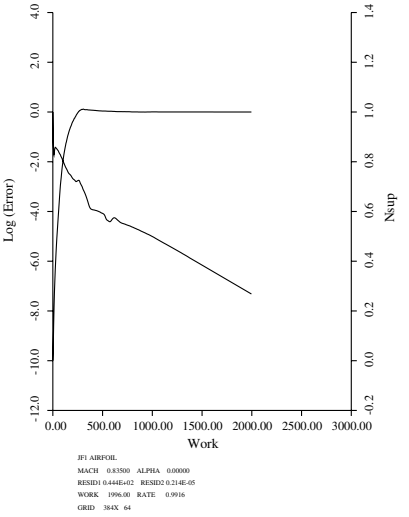

f) N-branch convergence history

Fig. 6 JF1 at Mach = 0.835 showing the symmetric solution (a) and convergence history (b), and the pair of asymmetric solutions (c and e) and convergence histories (d and f).

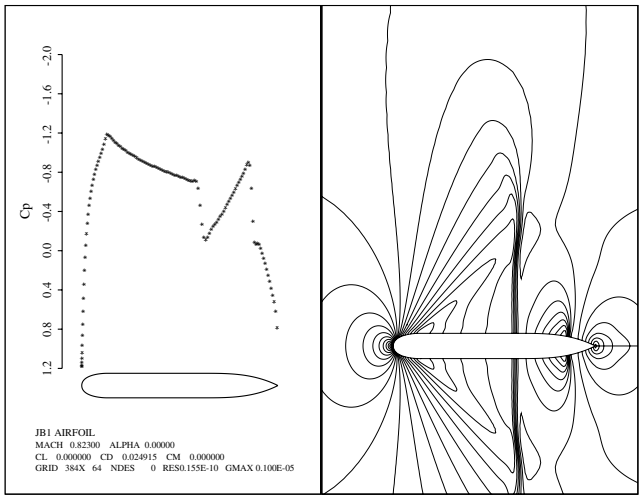

a) Z-branch Cp distribution and mach contours

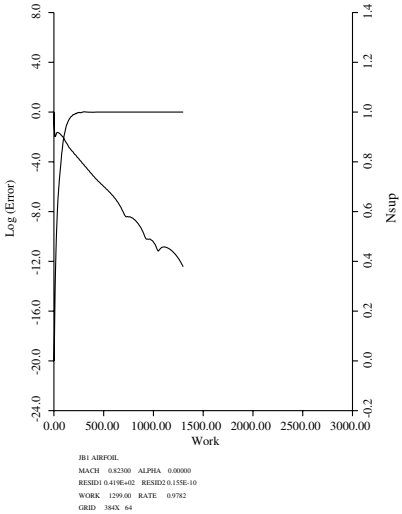

b) Z-branch convergence history

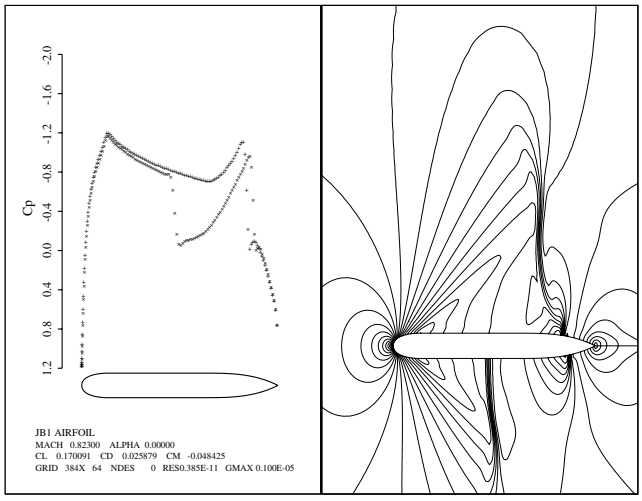

c) P-branch Cp distribution and mach contours

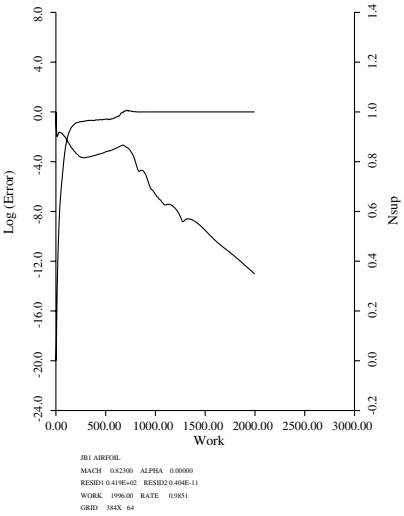

d) P-branch convergence history

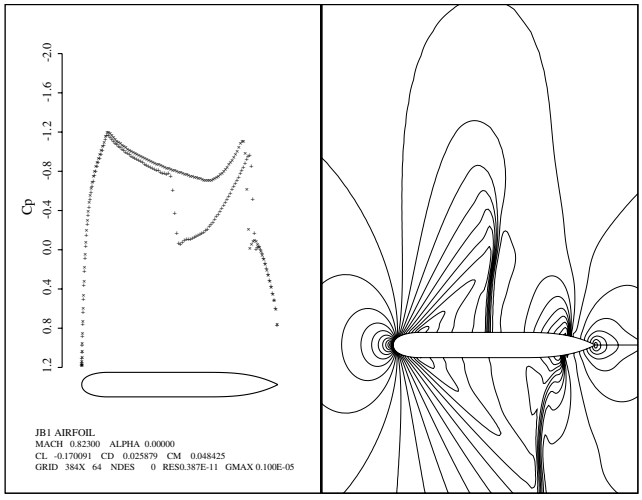

e) N-branch Cp distribution and mach contours

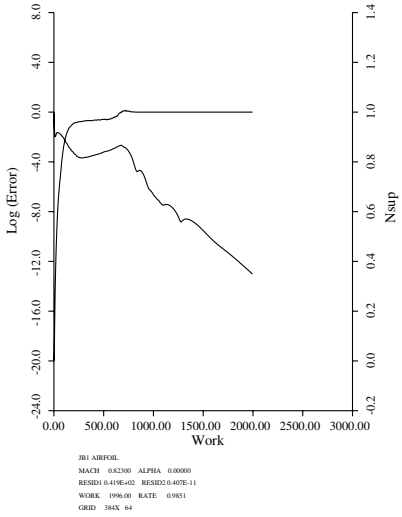

f) N-branch convergence history

Fig. 7 JB1 at Mach = 0.823 showing the symmetric solution (a) and convergence history (b), and the pair of asymmetric solutions (c and e) and convergence histories (d and f).

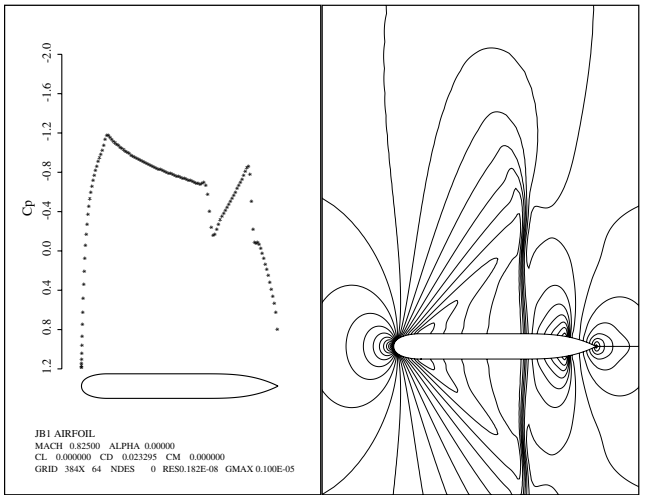

a) Z-branch Cp distribution and mach contours

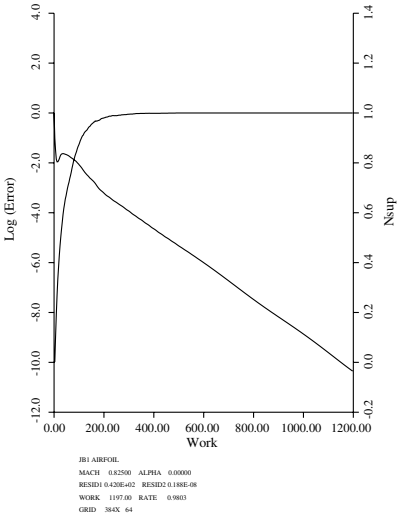

b) Z-branch convergence history

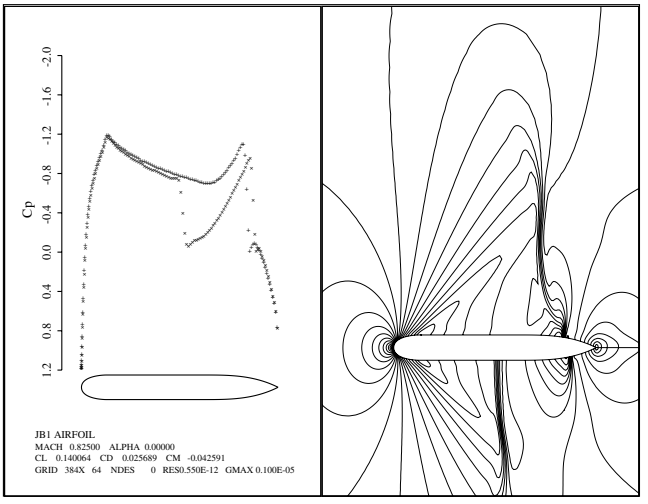

c) P-branch Cp Distribution and Mach Contours

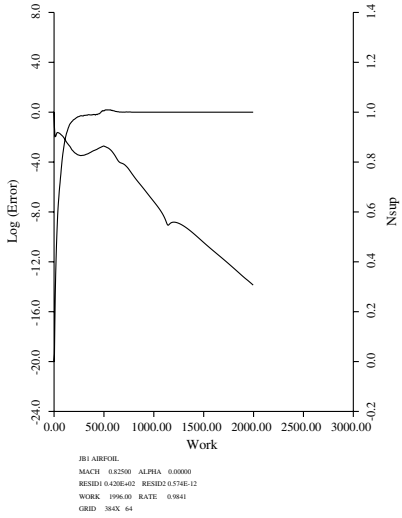

d) P-branch convergence history

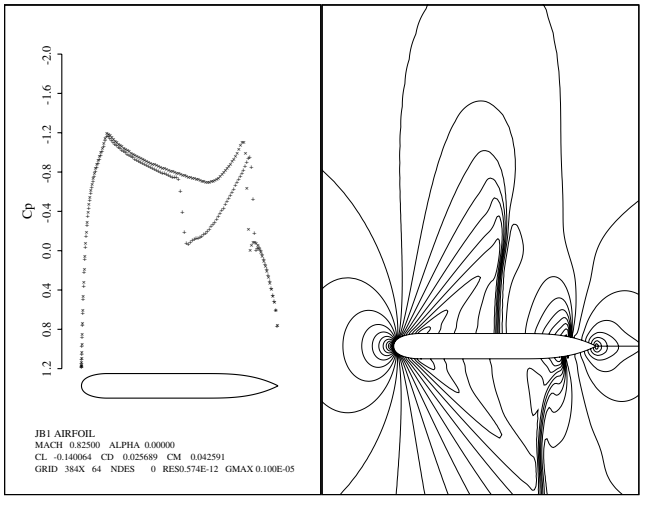

e) N-branch Cp distribution and mach contours

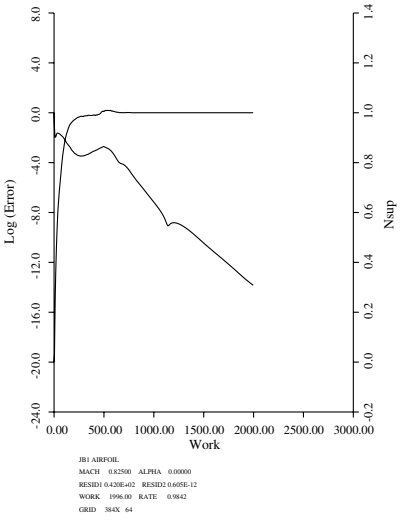

f) N-branch convergence history

Fig. 8 JB1 at Mach = 0.825 showing the symmetric solution (a) and convergence history (b), and the pair of asymmetric solutions (c and e) and convergence histories (d and f).

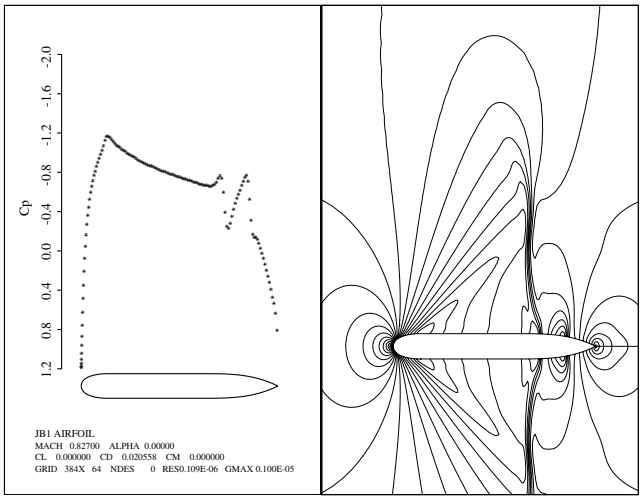

a) Z-branch Cp distribution and mach contours

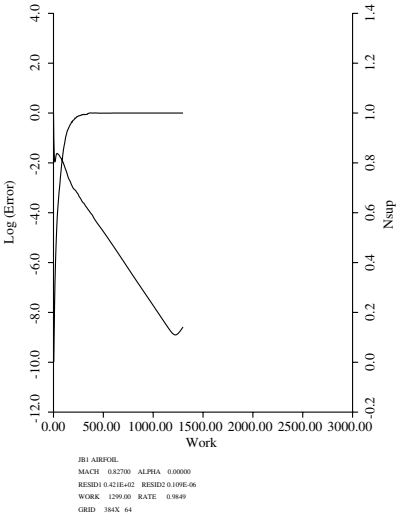

b) Z-branch convergence history

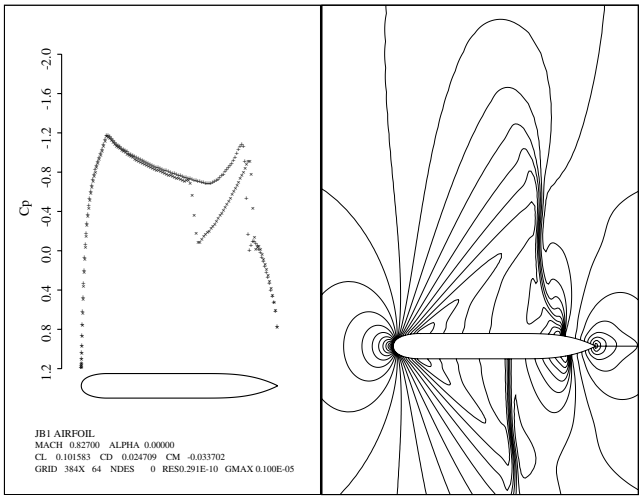

c) P-branch Cp distribution and mach contours

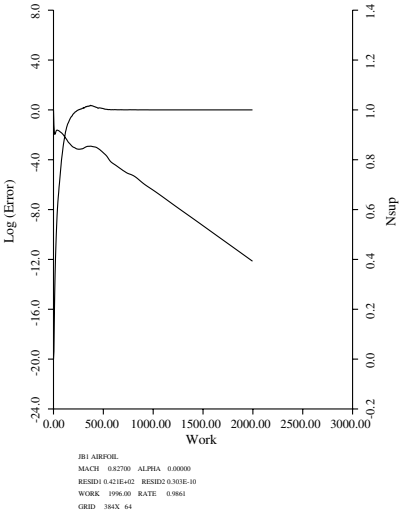

d) P-branch convergence history

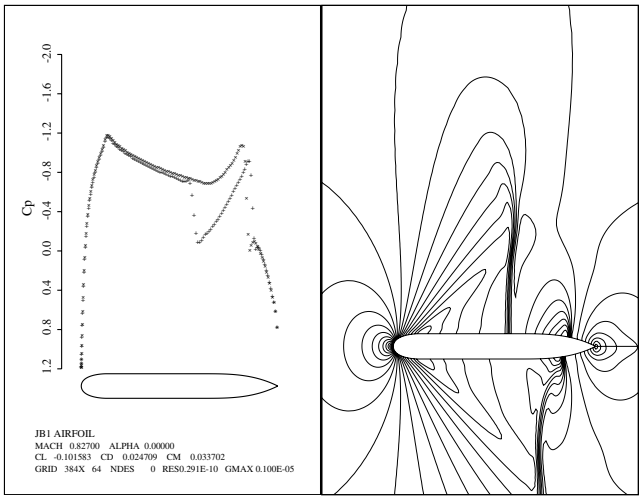

e) N-branch Cp distribution and mach contours

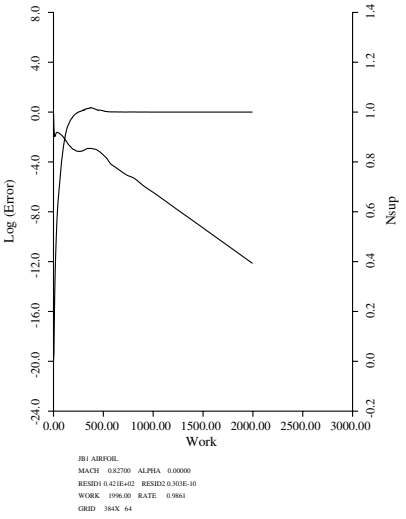

f) N-branch convergence history

Fig. 9 JB1 at Mach = 0.827 showing the symmetric solution (a) and convergence history (b), and the pair of asymmetric solutions (c and e) and convergence histories (d and f).

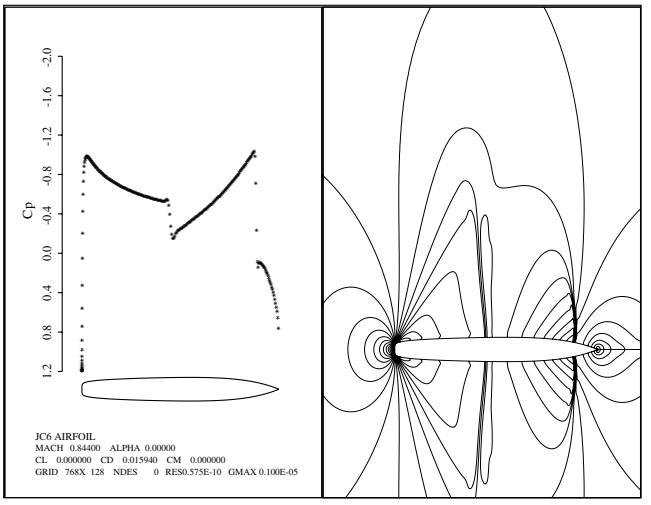

a) Z-branch Cp distribution and mach contours

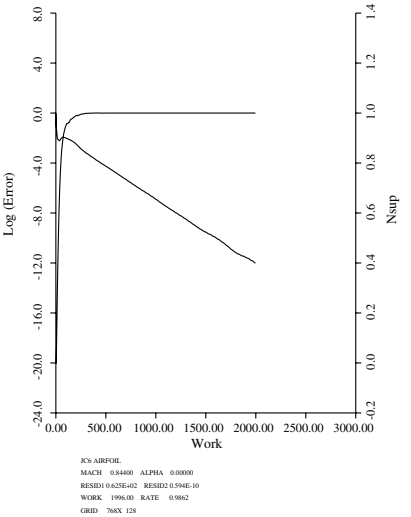

b) Z-branch convergence history

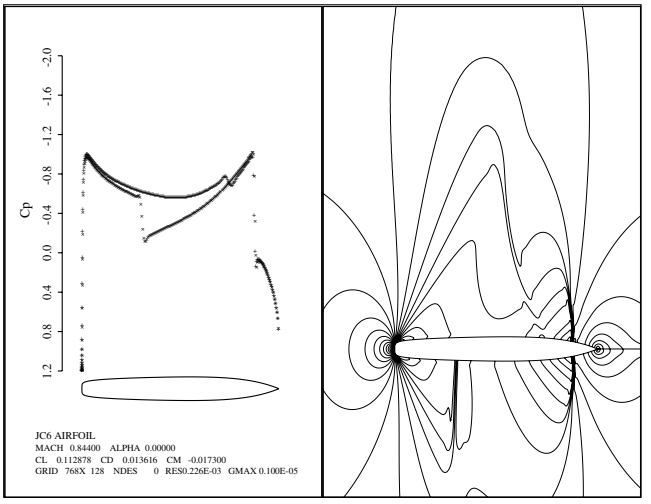

c) P-branch Cp distribution and mach contours

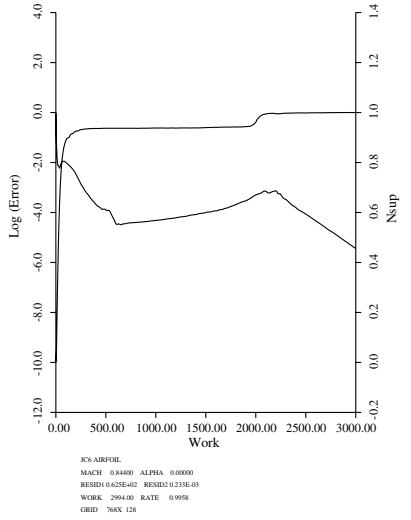

d) P-branch convergence history

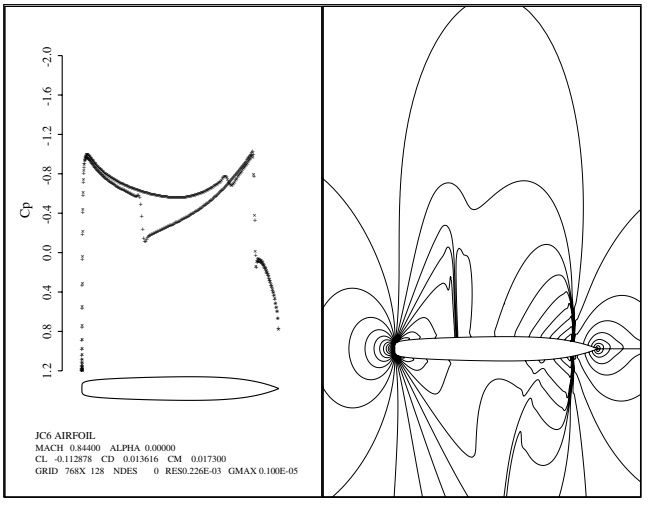

e) N-branch Cp distribution and mach contours

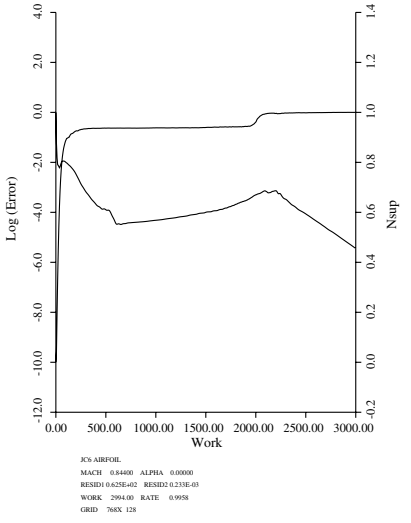

f) N-branch convergence history

Fig. 10 JC6 at Mach = 0.844 showing the symmetric solution (a) and convergence history (b), and the pair of asymmetric solutions (c and e) and convergence histories (d and f).

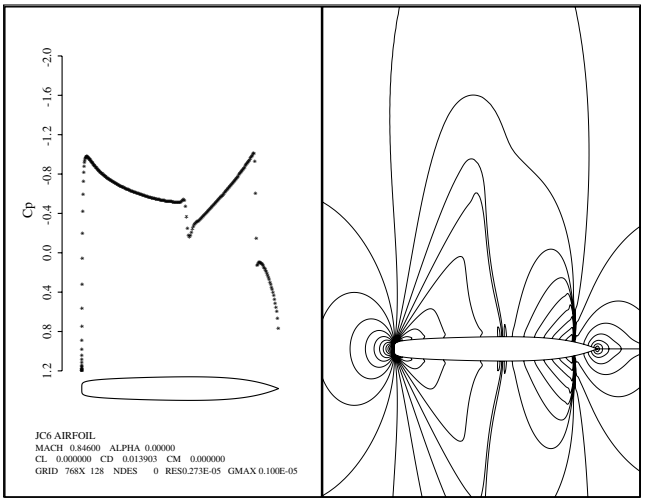

a) Z-branch Cp Distribution and Mach Contours

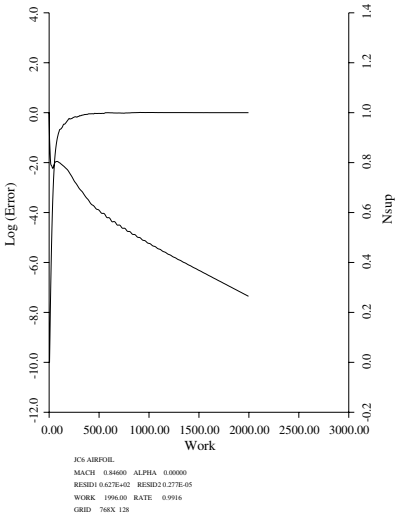

b) Z-branch convergence history

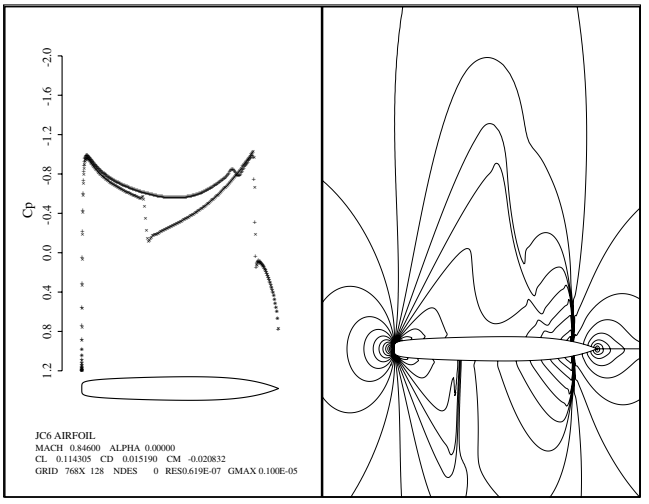

c) P-branch Cp distribution and mach contours

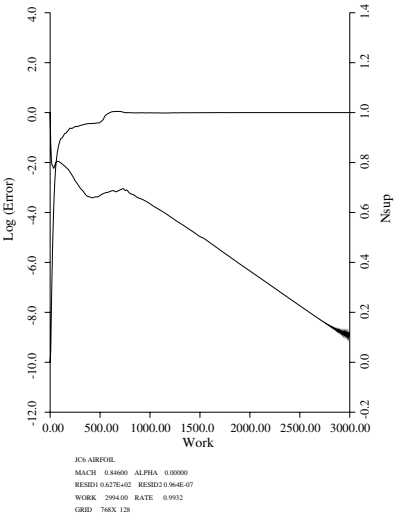

d) P-branch convergence history

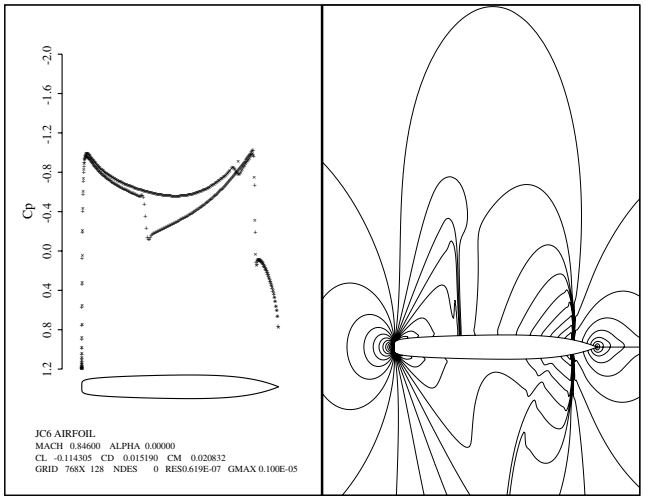

e) N-branch Cp distribution and mach contours

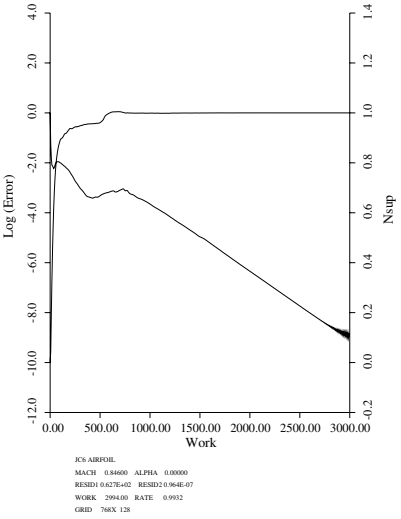

f) N-branch convergence history

Fig. 11 JC6 at Mach = 0.846 showing the symmetric solution (a) and convergence history (b), and the pair of asymmetric solutions (c and e) and convergence histories (d and f).

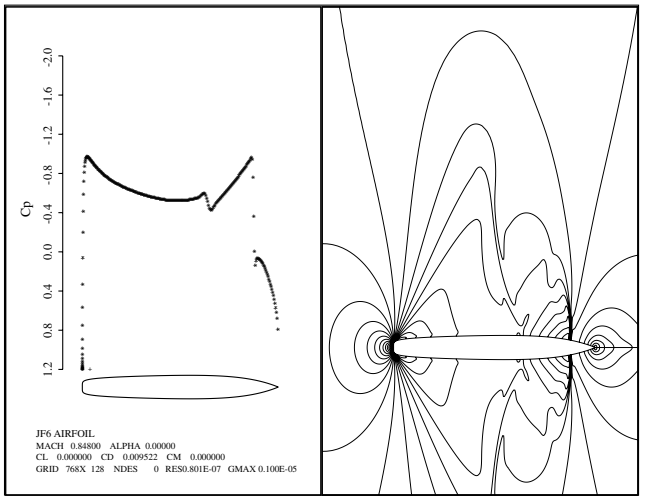

a) Z-branch Cp distribution and mach contours

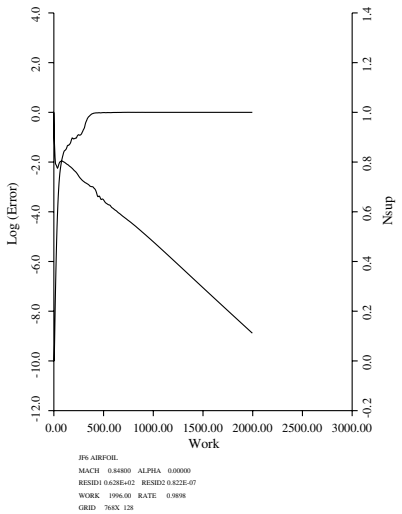

b) Z-branch convergence history

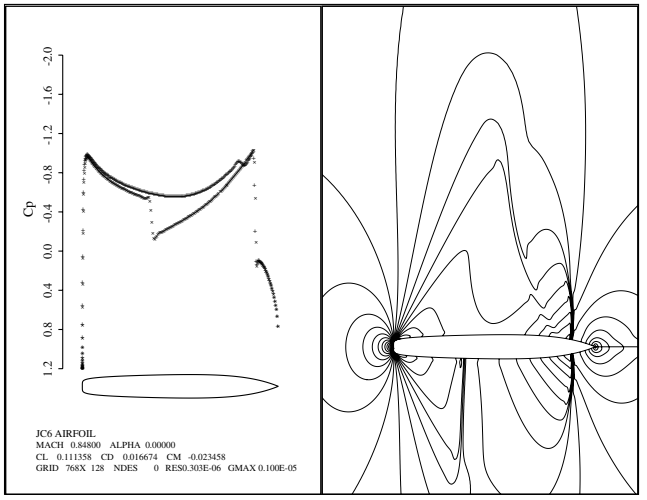

c) P-branch Cp distribution and mach contours

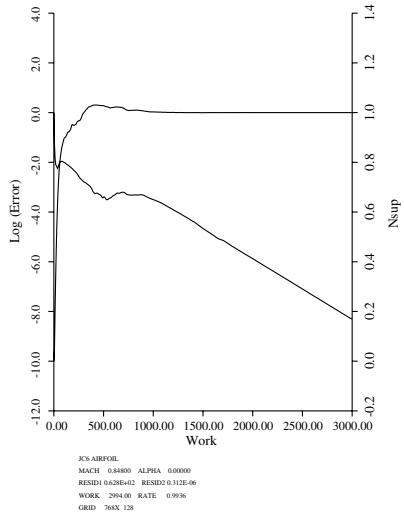

d) P-branch convergence history

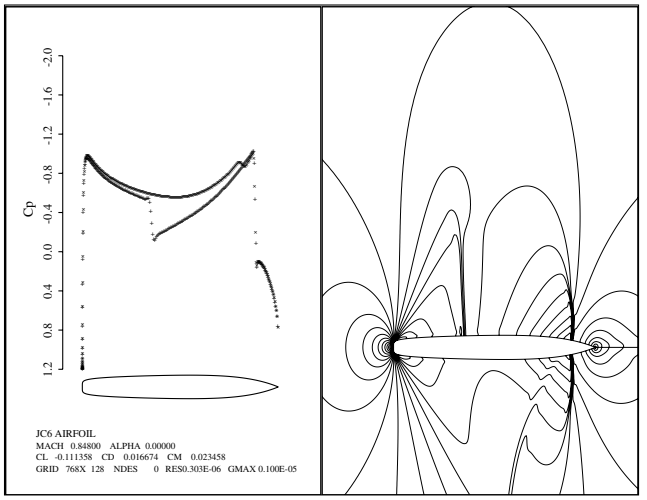

e) N-branch Cp distribution and mach contours

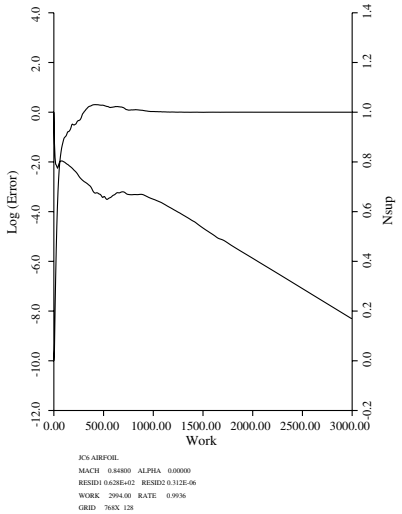

f) N-branch convergence history

Fig. 12 JC6 at Mach = 0.848 showing (a) the *z*-branch solution, (b) the *p*-branch solution, and (c) the *n*-branch solution.

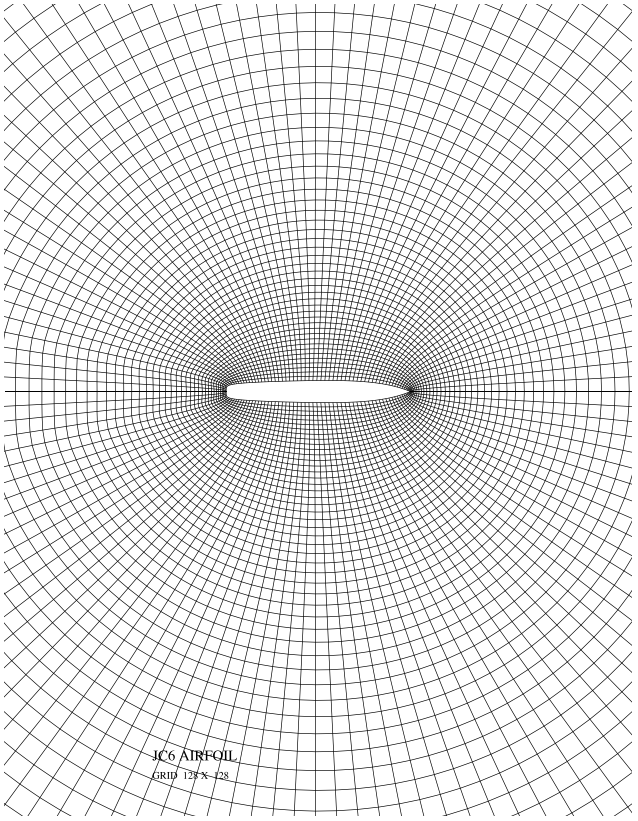

Fig. 13 A size 128 × 128 O-topology mesh used for the JC6 airfoil. Each mesh element has an unit aspect ratio.

simulations similar to those performed by Caughey [16] are needed to study the unsteady phenomenon of these transonic flows.

IV. Grid Convergence Study

A mesh refinement study was carried out to assess the discretization errors of the calculations performed in the present study. Because performing grid convergence studies for all the test cases is simply too much to undertake, we selected a representative case of the JC6 airfoil at Mach number 0.845 and at essentially 0 deg of angle of attack (0.0000001 deg). For this case, the lift coefficient is positive, i.e., it falls on the *P*-branch. The following four grid levels, 192×192, 256×256, 384×384, and 512×512, were used for studying grid convergence, but only the last three finest grid levels were used to establish the order of convergence and derive the asymptotic trendline. For each grid, the error residual was converged to machine-level-zero. The converged lift, drag, and moment coefficients for each grid level are tabulated and compared in Table 1 and displayed in Fig. 19 for the asymptotic range. Comparison is also made of the continuum estimates of the aerodynamic coefficients for the JC6 airfoil. The data in the table include estimates for the order-of-accuracy for each aerodynamic coefficient, as well as a Richardson extrapolation for each coefficient to its limiting value at the continuum where the grid width goes to zero. The generalized equation of computing the order of accuracy can be found in the recent work by Vassberg and Jameson [17]. It is presented here for completeness:

$$(F_f - F_m)h_c^p + (F_c - F_f)h_m^p + (F_m - F_c)h_f^p = 0$$

Here, F is the discrete functional computed on fine, medium, and coarse meshes of a family of grids, signified by subscripts f, m, and c, respectively. The length scale of the cells of a mesh is designated h, and the estimate of the order of accuracy is the power p.

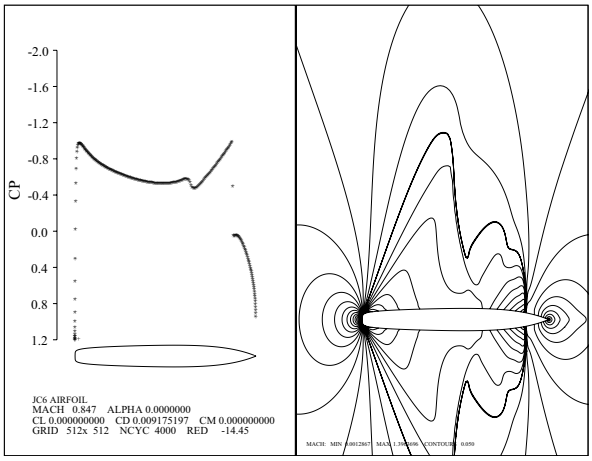

a) Z-branch Cp distribution and mach contours

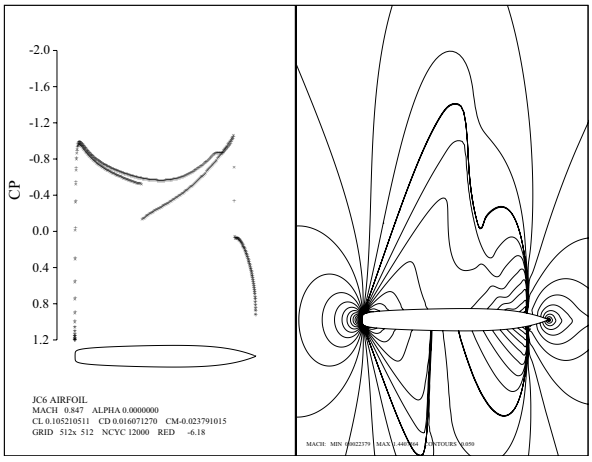

b) P-branch Cp distribution and mach contours

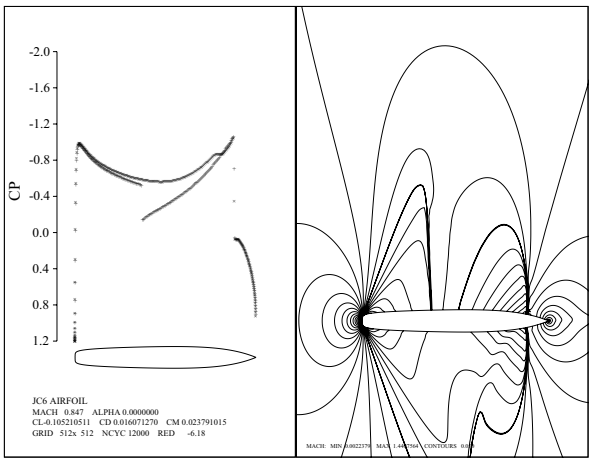

c) N-branch Cp distribution and mach contours

Fig. 14 JC6 at Mach = 0.847 showing (a) the *z*-branch solution, (b) the *p*-branch solution, and (c) the *n*-branch solution.

From the data we can see that the aerodynamic coefficients at the finest grid level have converged very close to the predicted continuum values. Even at the coarsest grid level, the solutions are sufficiently accurate for the purpose of the present study, which is to demonstrate that certain transonic flows can acquire non-unique solutions at a given angle of attack. We conclude that the discretization errors in the computations are small enough that the main findings of our paper are not a result of numerical artifacts. As a final note, the non-unique solutions were obtained on the JC6 airfoil

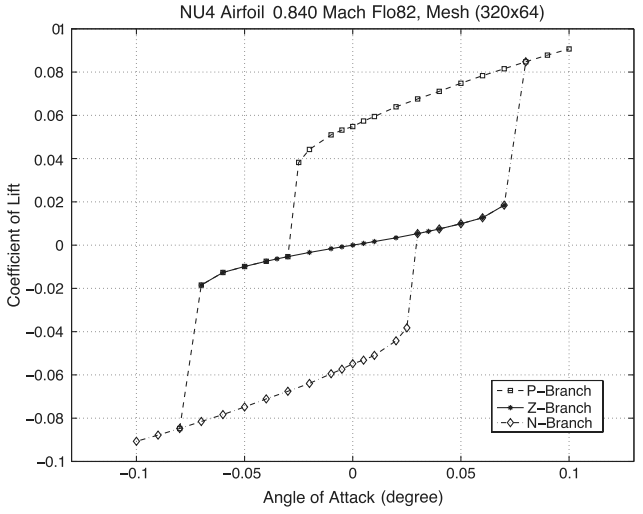

Fig. 15 $C_L - \alpha$ sweep for NU4 airfoil at Mach = 0.840.

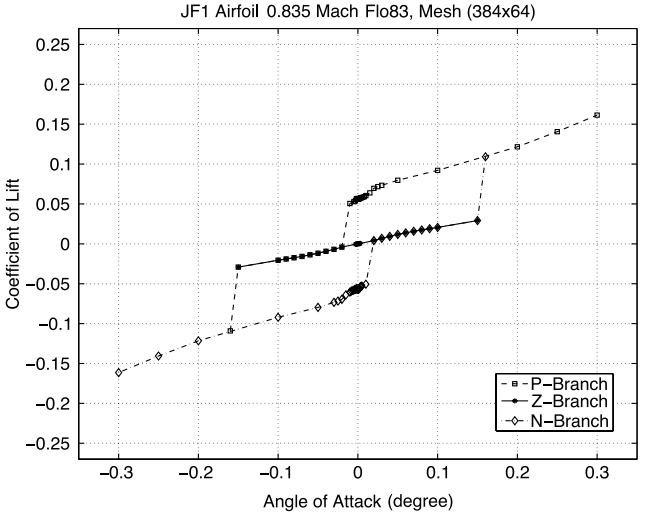

a) Full view of the (a) $C_L - \alpha$ sweep curve

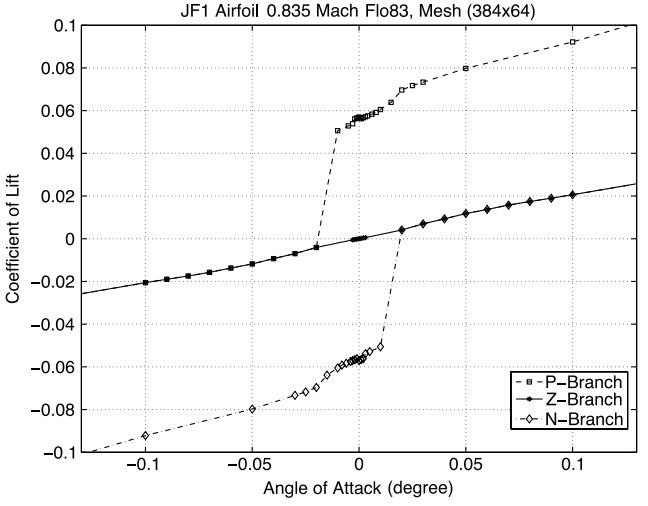

b) Zoom of the (a) $C_L - \alpha$ sweep curve near the Z-branch

Fig. 16 $C_L - \alpha$ sweep for JF1 airfoil at Mach = 0.835. Top figure displays the full view. Bottom figure is a zoom near the Z-branch.

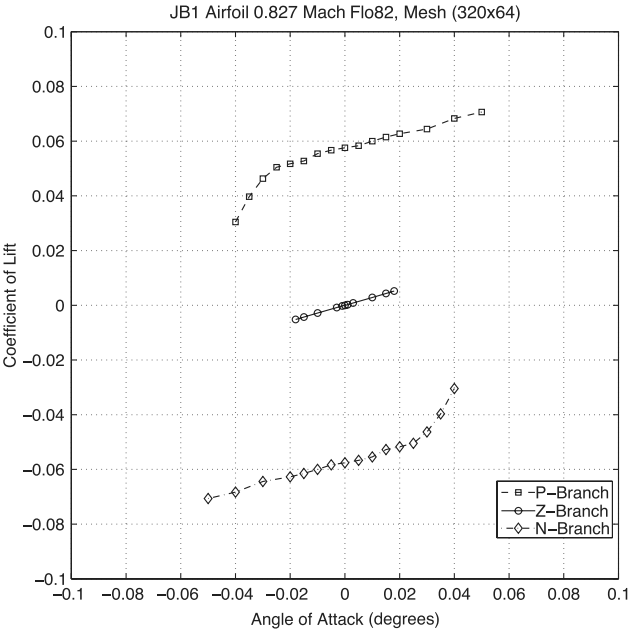

Fig. 17 $C_L - \alpha$ sweep for JB1 airfoil at Mach = 0.827.

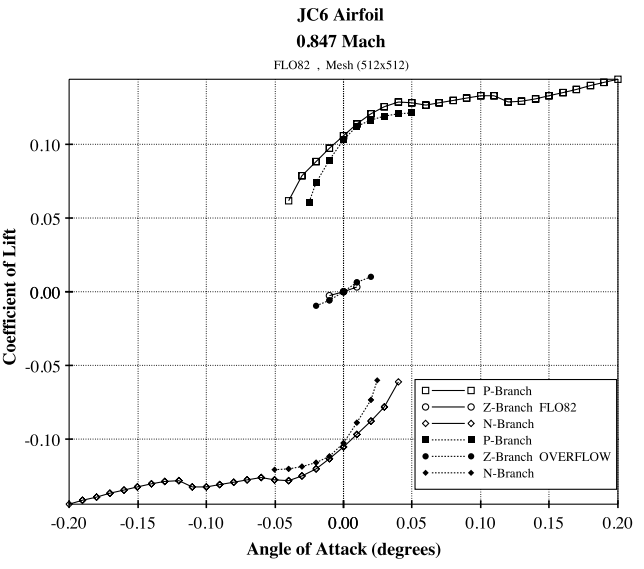

Fig. 18 $C_L - \alpha$ sweeps for JC6 airfoil at Mach = 0.847.

by multiple numerical solvers, which include FLO82, SYN83, and OVERFLOW, and on both C-mesh and O-mesh topologies. Therefore our current observation of non-uniqueness of transonic solution is not unique to an isolated solver.

Table 1 Grid convergence data for FLO82-HCUSP solutions of flows over a JC6 airfoil at Mach number 0.845 at 0 deg angle of attack

Grid	*h*-Ratio	*Cl*	*Cd*	*Cm*
192	2.667	0.103723589	0.016584893	−0.021532881
256	2.000	0.109588905	0.015630346	−0.022448422
384	1.333	0.103974085	0.014725021	−0.019766808
512	1.000	0.102967796	0.014508890	−0.019157914
Continuum	0.000	0.102467141	0.014355261	−0.018752871
p-Order		3.830	3.053	3.190

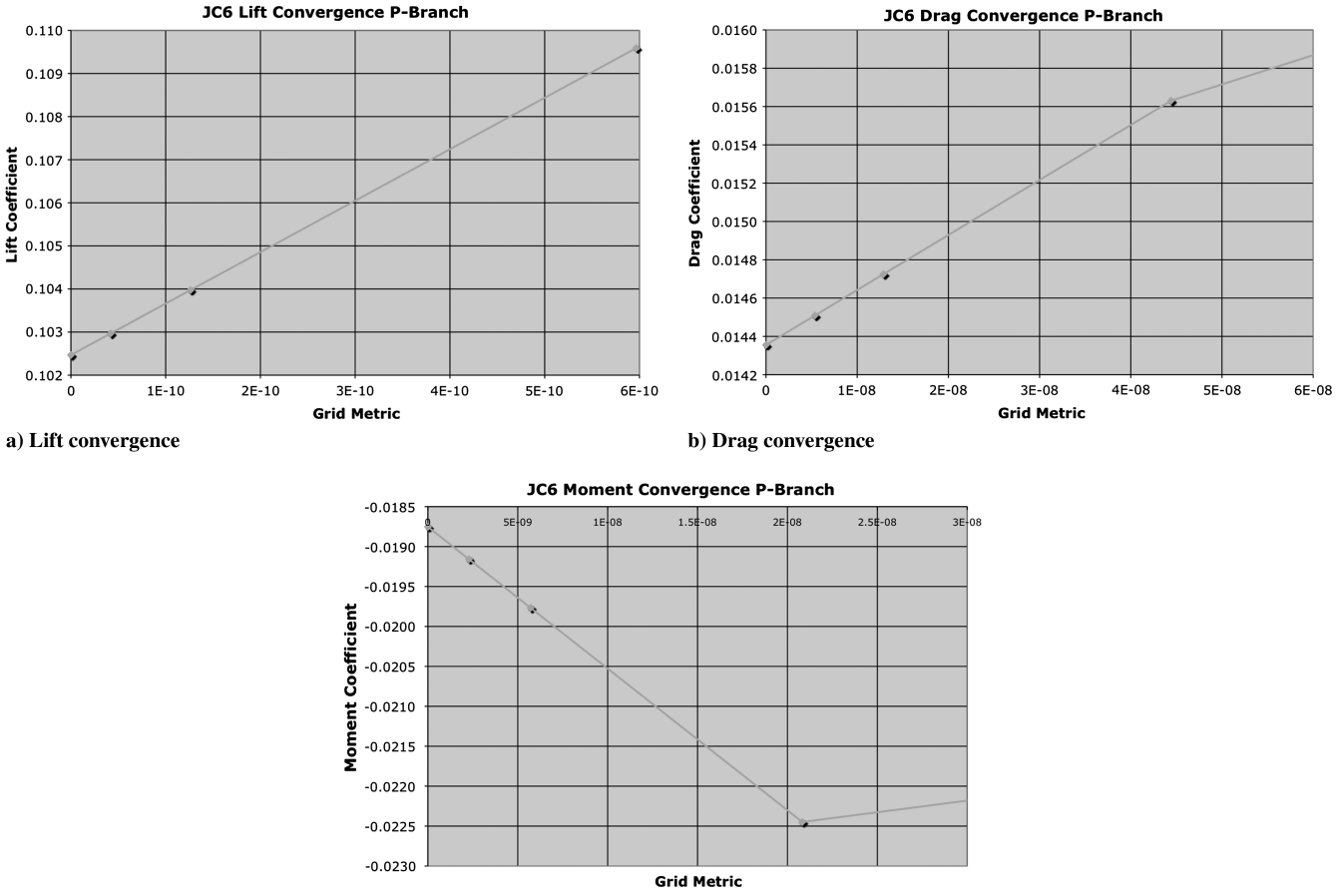

a) Lift convergence

b) Drag convergence

c) Moment convergence

Fig. 19 Grid convergences of the aerodynamic coefficients computed by FLO82-HCUSP scheme for flows over a JC6 airfoil at Mach 0.845 at zero angle of attack.

V. Conclusions

The results for these four very different airfoils exhibit a similar general pattern. They all have solutions that have a rather abrupt transition from two supersonic zones below a certain critical Mach number to a single supersonic zone above that Mach number. Non-uniqueness occurs in a range of Mach numbers between a point at which the two zones are quite widely spaced up to the point at which they coalesce. In this range, symmetric double shocked solutions appear to be unstable. Stable asymmetric solutions are found when two supersonic zones coalesce on one surface but not the other. When, for example, there are two supersonic zones on the lower surface the increase in pressure behind the first shock produces lift. The corresponding circulation then leads to an increase in the effective Mach number on the upper surface and a decrease on the lower surface, thus reinforcing the upper and lower surface solutions along the branches corresponding to single and double supersonic zones, respectively. This mechanism is not sufficient, however, to describe the behaviors of the original non-unique solutions for lifting airfoils reported by Jameson in 1991. Unsteady simulations are needed to gain a better understanding of the evolution and stability of these flows.

References

[1] Steinhoff, J., and Jameson, A., "Multiple Solution of the Transonic Potential Flow Equations," *AIAA Journal*, Vol. 20, No. 11, 1982, pp. 1521–1525. doi:10.2514/3.51216

[2] Salas, M. D., Melnik, R. E., and Jameson, A., "A Comparative Study of the Non-Uniqueness Problem of the Potential Equation," AIAA Paper 1983-1888, July 1983.

[3] Jameson, A., "Airfoil Admitting Non-Unique Solutions to the Euler Equations," AIAA Paper 1991-1625, June 1991.

[4] Hafez, M. M., and Guo, W. H., "Nonuniqueness of Transonic Flows," *Acta Mechanica*, Vol. 138, Nos. 3–4, 1999, pp. 177–184. doi:10.1007/BF01291843

[5] Hafez, M. M., and Guo, W. H., "Some Anomalies of Numerical Simulation of Shock Waves. Part I: Inviscid Flows," *Computers and Fluids*, Vol. 28, Nos. 4–5, 1999, pp. 701–719. doi:10.1016/S0045-7930(98)00051-6

[6] Hafez, M. M., and Guo, W. H., "Some Anomalies of Numerical Simulation of Shock Waves. Part II: Effect of Artificial and Real Viscosity," *Computers and Fluids*, Vol. 28, Nos. 4–5, 1999, pp. 721–739. doi:10.1016/S0045-7930(98)00052-8

[7] Kuz'min, A. G., and Ivanova, A. V., "The Structural Instability of Transonic Flow Associated with Amalgamation/Splitting of Supersonic Regions," *Theoretical and Computational Fluid Dynamics*, Vol. 18, No. 5, 2004, pp. 335–344. doi:10.1007/s00162-004-0145-1

[8] Kuz'min, A. G., "Instability and Bifurcation of Transonic Flow over Airfoils," AIAA Paper 2005-4800, June 2004.

[9] Ivanova, A. V., and Kuz'min, A. G., "Non-Uniqueness of the Transonic Flow Past an Airfoil," *Fluid Dynamics*, Vol. 39, No. 4, 2004, pp. 642–648. doi:10.1023/B:FLUI.0000045680.74521.80

[10] Kuz'min, A. G., "Bifurcation of Transonic Flow over a Flattened Airfoil," *Frontiers of Computational Fluid Dynamics*, World Scientific Publishing Company Ltd., Hackensack, NJ, 2006, pp. 285–291.

[11] Kuz'min, A. G., "Structural Instability of Transonic Flow over an Airfoil," *Journal of Engineering Physics and Thermophysics*, Vol. 77, No. 5, 2004, pp. 1022–1026. doi:10.1023/B:JOEP.0000049545.65787.74

[12] Vassberg, J. C., Harrison, N. A., Roman, D. L., and Jameson A., "Systematic Study on the Impact of Dimensionality for a Two-Dimensional Aerodynamic Optimization Model Problem," AIAA Paper 2011-3176, 29 June 2011.

[13] Jameson, A., Schmidt, W., and Turkel, E., "Numerical Solutions of the Euler Equations by Finite Volume Methods Using Runge-Kutta Time-

Stepping Schemes," AIAA Paper 1981-1259, June 1981.
[14] Jameson, A., "Analysis and Design of Numerical Schemes for Gas Dynamics 2 Artificial Diffusion and Discrete Shock Structure," *International Journal of Computational Fluid Dynamics*, Vol. 5, Nos. 1–2, 1995, pp. 1–38. doi:10.1080/10618569508940734
[15] Buning, P. G., Jespersen, D. C., Pulliam, T. H., Klopfer, G. H., Chan, W. M., Slotnick, J. P., Krist, S. E., and Renze, K. J., OVERFLOW User's Manual, Version 1.8L, NASA, July 1999.
[16] Caughey, D. A., "Stability of Unsteady Flow Past Airfoils Exhibiting Transonic Non-Uniqueness," *Computational Fluid Dynamics Journal*, Vol. 13, No. (3):60, 2004, pp. 427–438.
[17] Vassberg, J. C., and Jameson, A. "In Pursuit of Grid Convergence, Part I: Two-Dimensional Euler Solutions," *Journal of Aircraft*, Vol. 47, No. 4, 2010; also AIAA Paper 2009-4114, June 2009. doi:10.2514/1.46737

W. K. Anderson
Associate Editor